

This copy is for your personal, non-commercial use only.

If you wish to distribute this article to others, you can order high-quality copies for your colleagues, clients, or customers by [clicking here](#).

Permission to republish or repurpose articles or portions of articles can be obtained by following the guidelines [here](#).

The following resources related to this article are available online at www.sciencemag.org (this information is current as of October 25, 2010):

Updated information and services, including high-resolution figures, can be found in the online version of this article at:

<http://www.sciencemag.org/cgi/content/full/329/5996/1175>

Supporting Online Material can be found at:

<http://www.sciencemag.org/cgi/content/full/329/5996/1175/DC1>

A list of selected additional articles on the Science Web sites **related to this article** can be found at:

<http://www.sciencemag.org/cgi/content/full/329/5996/1175#related-content>

This article **cites 41 articles**, 10 of which can be accessed for free:

<http://www.sciencemag.org/cgi/content/full/329/5996/1175#otherarticles>

This article has been **cited by 1** articles hosted by HighWire Press; see:

<http://www.sciencemag.org/cgi/content/full/329/5996/1175#otherarticles>

This article appears in the following **subject collections**:

Microbiology

<http://www.sciencemag.org/cgi/collection/microbio>

Spiroindolones, a Potent Compound Class for the Treatment of Malaria

Matthias Rottmann,^{1,2*} Case McNamara,^{3*} Bryan K. S. Yeung,^{4*} Marcus C. S. Lee,⁵ Bin Zou,⁴ Bruce Russell,^{6,7} Patrick Seitz,^{1,2} David M. Plouffe,³ Neekesh V. Dharia,⁸ Jocelyn Tan,⁴ Steven B. Cohen,³ Kathryn R. Spencer,⁸ Gonzalo E. González-Páez,⁸ Suresh B. Lakshminarayana,⁴ Anne Goh,⁴ Rossarin Suwanarusk,⁶ Timothy Jegla,⁹ Esther K. Schmitt,¹⁰ Hans-Peter Beck,^{1,2} Reto Brun,^{1,2} Francois Nosten,^{11,12,13} Laurent Renia,⁶ Veronique Dartois,⁴ Thomas H. Keller,⁴ David A. Fidock,^{5,14} Elizabeth A. Winzeler,^{3,8†} Thierry T. Diagana^{4*†}

Recent reports of increased tolerance to artemisinin derivatives—the most recently adopted class of antimalarials—have prompted a need for new treatments. The spiroetrahydro- β -carboline, or spiroindolones, are potent drugs that kill the blood stages of *Plasmodium falciparum* and *Plasmodium vivax* clinical isolates at low nanomolar concentration. Spiroindolones rapidly inhibit protein synthesis in *P. falciparum*, an effect that is ablated in parasites bearing nonsynonymous mutations in the gene encoding the P-type cation-transporter ATPase4 (PfATP4). The optimized spiroindolone NITD609 shows pharmacokinetic properties compatible with once-daily oral dosing and has single-dose efficacy in a rodent malaria model.

Almost half the world's population is exposed to malaria, which causes over 800,000 deaths each year and kills more under-5-year-olds than any other infectious agent (1). Fifty years ago, malaria had been eliminated from many areas of the world through a combination of drug treatments and vector control interventions (2). However, the global spread of drug resistance together with a collapse of vector control programs resulted, by the 1980s, in a resurgence in disease incidence and mortality. Today, epidemiological data suggest that the introduction of new drugs (notably the artemisinin-based combination therapies or ACTs) may have reversed that trend (3). Recent reports suggest that resistance to derivatives of the endoperoxide artemisinin is now emerging (4–6). These observations have triggered a concerted search for new drugs that could be deployed if artemisinin resistance were to spread.

Many of the therapies currently in development use known antimalarial pharmacophores (e.g., aminoquinolines and/or peroxides) chemically modified to overcome the liabilities of their predecessors (7). Although these compounds may become important in the treatment of malaria, it would be preferable to discover chemotypes with novel mechanisms of actions (8). However, despite important advances in our understanding of the *Plasmodium* genome, the identification and validation of new drug targets have been challenging (9).

To identify novel antimalarial leads, we and others have screened diverse chemical libraries using *Plasmodium* whole-cell proliferation assays with cultured intraerythrocytic parasites (10–12). From a library of about 12,000 pure natural products and synthetic compounds with structural features found in natural products, our screen identified 275 primary hits with submicromolar activity against *Plasmodium falciparum*. We discarded those hits whose activity was not reconfirmed against multidrug-resistant parasites and/or that displayed some cytotoxicity against mammalian cells (more than 50% viability inhibition at 10 μ M). Pharmacokinetic and physical properties were then determined for the remaining 17 compounds. From this, a synthetic compound related to the spiroazepineindole class, having a favorable pharmacological profile, stood out as a starting point for a medicinal chemistry lead optimization effort. Synthesis and evaluation of about 200 derivatives yielded the optimized spiroetrahydro- β -carboline (or spiroindolone) compound NITD609 (Fig. 1A). This compound is synthesized in eight steps, including chiral separation of the active enantiomer, and is amenable to large-scale manufacturing. NITD609 has good drug-like attributes (see below) and displays physicochemical properties compatible with conventional tablet formulation.

There is general agreement that a new antimalarial should ideally meet the following criteria: (i) kills parasite blood stages; (ii) is active against

drug-resistant parasites; (iii) is safe (i.e., no cytotoxicity, genotoxicity, and/or cardiotoxicity); and (iv) has pharmacokinetic properties compatible with once-daily oral dosing. NITD609 meets all these criteria. We also gained insight into a mechanism of drug resistance involving the P-type cation-transporter ATPase4 (PfATP4).

Activity against drug-resistant *Plasmodium*. Antimalarial blood-stage activity was evaluated in vitro against a panel of culture-adapted *P. falciparum* strains. NITD609 displayed single-digit nanomolar average 50% inhibitory concentration values (IC₅₀ range, 0.5 to 1.4 nM; table S1), with no evidence of diminished potency against drug-resistant strains (table S1) (13). This compound was also tested in ex vivo assays with fresh isolates of *P. falciparum* and *P. vivax* (14), collected from malaria patients on the Thai-Burmese border where chloroquine resistance has been widely reported (15, 16). NITD609 was found to be as effective as artesunate, with potency in the low nanomolar range (IC₅₀ values consistently <10 nM) against all *P. vivax* (Fig. 1B) and *P. falciparum* (Fig. 1C) isolates. NITD609 was also similar to artesunate in its ability to kill both mature trophozoite and immature *P. vivax* ring stages, in contrast to the trophozoite stage-specific activity observed with chloroquine (17). Regardless of their initial developmental stages, NITD609-treated parasites displayed morphological hallmarks of dying parasites, including pycnotic nuclei and abnormal digestive vacuoles and/or nuclear segmentation. Collectively, our in vitro and ex vivo data showed that spiroindolones were potent against the intraerythrocytic stages of the major human malarial pathogens *P. falciparum* and *P. vivax*, including a range of drug-resistant strains.

The rapid activity of artemisinin derivatives against all *Plasmodium* asexual erythrocytic stages is a key feature of their therapeutic efficacy (6). To precisely determine which parasite blood stages are most sensitive to the spiroindolones, and to evaluate the time required for these drugs to act, we conducted in vitro drug sensitivity assays with synchronized parasites treated at ring, trophozoite, and schizont stages for various durations (1, 6, 12, and 24 hours) before removal of drug and continuation of culture for 24 hours in the presence of [³H]hypoxanthine. At a high concentration of NITD609 ($\approx 100 \times$ IC₅₀ value), all stages (rings, trophozoites, and schizonts) were similarly sensitive (fig. S1). However, at low concentrations (≈ 1 or $10 \times$ IC₅₀ value), schizonts were the most susceptible. We speculate that the target is present in all asexual blood stages but might be particularly vulnerable in schizonts. Although clearly faster-acting than the former first-line antifolate agent pyrimethamine, NITD609 did not inhibit parasite growth as quickly as the artemisinin derivative artemether (fig. S1). Strong growth inhibition (>90%) was achieved with artemether treatment at 8 nM for only 6 hours, whereas similar activity was achieved with NITD609 at 1.6 nM for 24 hours.

Although at least 12 hours of continuous drug exposure was required to reduce by 90% the in-

¹Swiss Tropical and Public Health Institute, Parasite Chemotherapy, CH-4002 Basel, Switzerland. ²University of Basel, CH-4003 Basel, Switzerland. ³Genomics Institute of the Novartis Research Foundation, San Diego, CA 92121, USA. ⁴Novartis Institute for Tropical Diseases, 138670 Singapore. ⁵Department of Microbiology and Immunology, Columbia University Medical Center, New York, NY 10032, USA. ⁶Laboratory of Malaria Immunobiology, Singapore Immunology Network, Agency for Science Technology and Research (A*STAR), Biopolis, 138648, Singapore. ⁷Department of Microbiology, National University of Singapore, 117597, Singapore. ⁸Department of Cell Biology, The Scripps Research Institute, La Jolla, CA 92037, USA. ⁹Department of Biology and Huck Institute of Life Sciences, Pennsylvania State University, University Park, PA 16802, USA. ¹⁰Natural Products Unit, Novartis Pharma AG, CH-4002 Basel, Switzerland. ¹¹Shoklo Malaria Research Unit, Mae Sot, Tak 63110, Thailand. ¹²Faculty of Tropical Medicine, Mahidol University, Bangkok, Thailand. ¹³Centre for Tropical Medicine, Nuffield Department of Clinical Medicine, University of Oxford, Oxford OX3 7JL, UK. ¹⁴Department of Medicine (Division of Infectious Diseases), Columbia University Medical Center, New York, NY 10032, USA.

*These authors contributed equally to this work.

†To whom correspondence should be addressed. E-mail: winzeler@scripps.edu (E.A.W.); thierry.diagana@novartis.com (T.T.D.)

corporation of [^3H]-hypoxanthine into parasite DNA (fig. S1), a [^{35}S]-radiolabeled methionine and cysteine ([^{35}S]-Met/Cys) incorporation assay revealed that NITD609 blocked protein synthesis in *P. falciparum* parasites within 1 hour (Fig. 2A). A similar effect was observed with the known protein translation inhibitors anisomycin (an inhibitor of peptidyl transferase) and cycloheximide (an inhibitor of translocation activities during polypeptide elongation). In contrast, the antimalarial drugs artemisinin and mefloquine showed a nom-

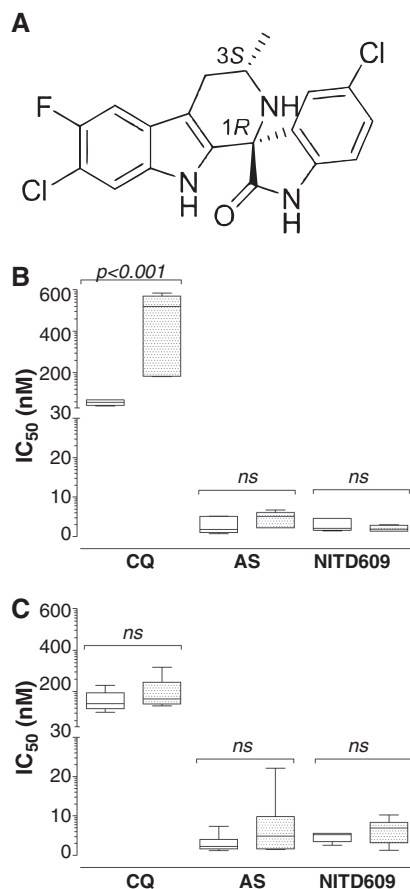
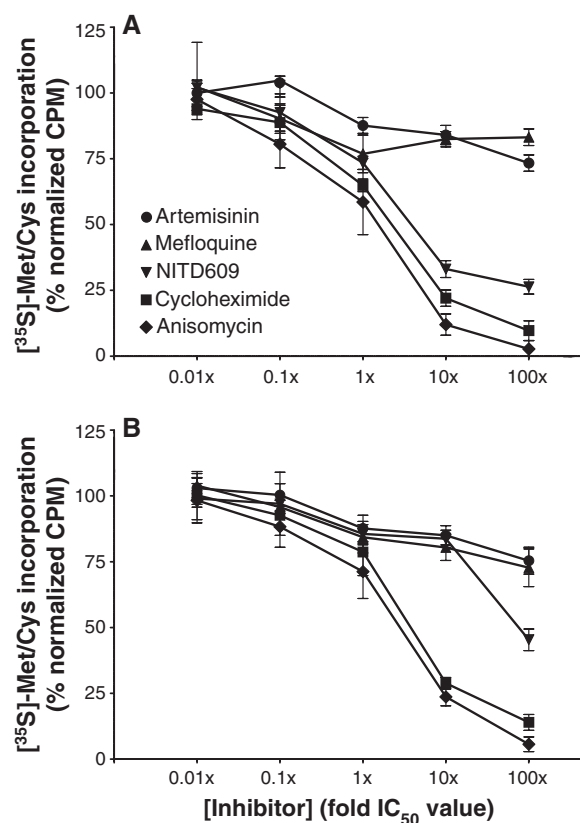


Fig. 1. (A) Chemical structure of NITD609, showing the 1R,3S configuration that is essential for antimalarial activity. Key physicochemical properties: solubility (pH 6.8), 39 $\mu\text{g}/\text{ml}$; logP (pH 7.4), 4.7; logD (pH 7.4), 4.6; pK_a^1 , 4.7; pK_a^2 , 10.7; polar surface area, 56.92 \AA^2 . (B) Ex vivo sensitivity of *P. vivax* and (C) *P. falciparum* (9 and 10 clinical isolates, respectively) to NITD609 compared with the reference drugs chloroquine (CQ) and artesunate (AS). The antimalarial sensitivity of these two species was measured after exposing ring (unshaded boxes) and trophozoite stages (shaded boxes) to drug for 20 hours. Data are shown as box plots. Maximum-minimum IC_{50} values are indicated, respectively, by the top and bottom horizontal thin bars, with the solid internal line indicating the median. Boxed areas indicate 75% confidence intervals. Inhibition of parasite growth was determined after 42 hours. Only chloroquine-treated *P. vivax* displayed a significant stage-specific sensitivity ($P < 0.001$). ns, not significant.

inal (<25%) decrease in [^{35}S]-Met/Cys incorporation within 1 hour. We suggest that NITD609 has a mechanism of action different from those of artemisinin and mefloquine.

Selectivity index and safety profile. Safety is paramount when considering that the malaria patient population is composed mostly of young children living in places where there are very limited resources for providing adequate medical supervision. To assess the intrinsic cytotoxic activity of NITD609, we measured the concentration leading to 50% cell death (CC_{50}) in vitro with cell lines of neural, renal, hepatic, or monocytic origin. No significant cytotoxicity was observed at any concentration ($\text{CC}_{50} > 10 \mu\text{M}$; table S2). Given that NITD609 had an IC_{50} of $\sim 1 \text{ nM}$ against *P. falciparum* (table S1), the cytotoxicity data established a selectivity index ($\text{CC}_{50}/\text{IC}_{50}$) $> 10,000$. Multiple antimalarial drugs (e.g., 4-aminoquinolines) have cardiotoxicity liabilities due to hERG channel inhibition, resulting in withdrawal in the extreme case of halofantrine (18, 19). hERG (human Ether-a-go-go Related Gene) binding and patch-clamp assays with NITD609 yielded IC_{50} values $> 30 \mu\text{M}$, consistent with a low risk of cardiotoxicity (table S3). Using a miniaturized Ames assay (20), we also established that NITD609 lacked intrinsic mutagenic activity. Finally, we observed no significant binding with a panel of human G-protein coupled receptors, enzymes, and ion channels (table S4).

Fig. 2. Spiroindolones rapidly diminish protein synthesis in the parasite. The rate of parasite protein synthesis was evaluated by monitoring [^{35}S]-radiolabeled methionine and cysteine ([^{35}S]-Met/Cys) incorporation into asynchronous cultures. Parasites were assayed for 1 hour in the presence of NITD609 (inverted triangle), anisomycin (diamond), cycloheximide (square), artemisinin (circle), or mefloquine (triangle), then extracted for radiographic measurements. Radiolabel incorporation was measured against inhibitor dosed over a five-log concentration range, and percent incorporation was calculated by comparison to cultures assayed in the absence of inhibitor. Anisomycin and cycloheximide were included as positive controls. (A) Spiroindolone treatment rapidly diminishes protein synthesis in Dd2; however, this effect is mostly absent in (B) NITD609- R^{Dd2} clone #2 except at very high concentration. Fifty percent inhibition of [^{35}S]-Met/Cys incorporation was observed with 3 \times and 78 \times IC_{50} of NITD609 on the NITD609-treated Dd2 wild type and NITD609- R^{Dd2} drug-resistant clones, respectively. Data are expressed as means \pm SD and represent three independent experiments performed in triplicate. Similar losses of protein synthesis inhibition upon NITD609 treatment were observed in the resistant clones NITD609- R^{Dd2} #1 and #3, respectively (see fig. S2).



Male rats tolerated oral administration of NITD609 daily for 14 days at a dose yielding daily exposure ($\text{AUC}_{0-24\text{h}}$) values between 29,400 and 56,500 ng-hour/ml. This is equivalent to 10- to 20-fold the daily exposure to a dose that reduced parasitemia by 99% in a malaria mouse model [99% effective dose (ED_{99}) = 5.3 mg/kg; see below]. Under these conditions, no adverse events or notable histopathological findings were observed. Overall, these data show that NITD609 has a safety profile that is acceptable for an antimalarial drug.

Pharmacokinetic and pharmacodynamic properties. Upon oral and intravenous administration in mice and rats, NITD609 displayed a moderate volume of distribution ($V_{ss} = 2.11$ and 3.04 liter/kg) and a low total systemic clearance ($\text{CL} = 9.75$ and 3.48 $\text{ml min}^{-1} \text{kg}^{-1}$) (table S5). Orally administered NITD609 displayed a long half-life ($T_{1/2} = 10$ and 27.7 hours) and excellent bioavailability ($F = 100\%$). On the basis of our in vitro metabolic stability data, this profile is likely to extend to humans, because the predicted metabolic clearance for this compound was low across several species (table S6). Taken together, these data show that NITD609 displays pharmacokinetic properties consistent with once-daily oral dosing. We tested this drug candidate by oral dosing in a virulent *P. berghei* malaria mouse model (21, 22). The results showed that

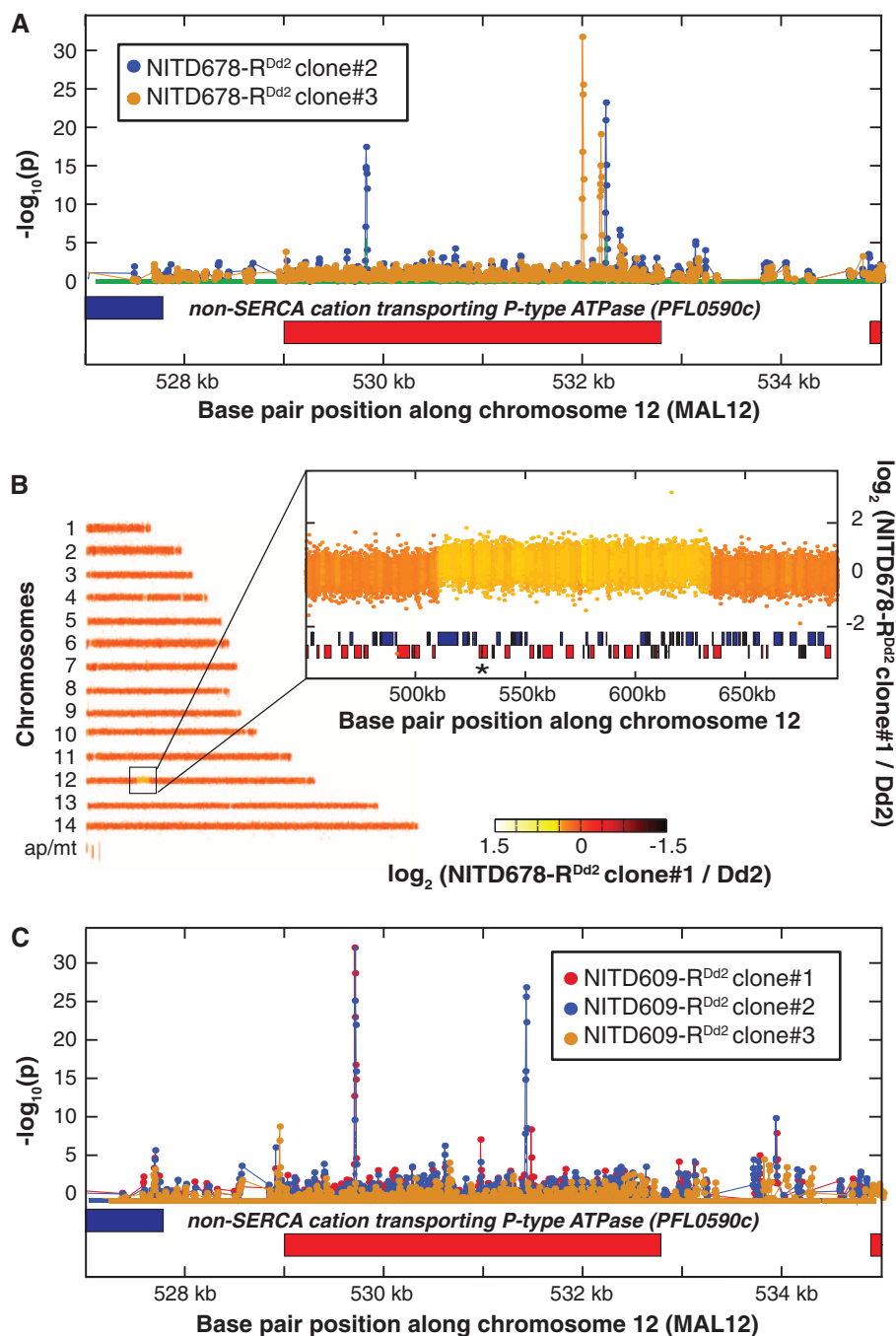
Table 1. In vivo efficacy data in the *P. berghei* rodent malaria model. "Activity": average parasitemia reduction; "Survival": average life span after infection (6 to 7 days for untreated mice); "Cure": no parasite present at day 30.

Compound	1 × 10 mg/kg oral		1 × 30 mg/kg oral			1 × 100 mg/kg oral		
	Activity (%)	Survival (%)	Activity (%)	Survival (days)	Cure (%)	Activity (%)	Survival (days)	Cure (%)
NITD609*	99.6	13.3	99.6	24.1	50	99.2	>30	100
Artesunate [†]	70	7.3	89	7.2	—	97	6.7	—
Artemether [†]	81	6.2	97	6.9	—	99	7.6	—
Chloroquine [†]	99.6	8	99.7	8.7	—	>99.9	12	—
Mefloquine [†]	95	15.2	98	18.2	—	89	28	—

*Methylcellulose 0.5%/0.1% Solutol HS15 formulation ($n = 10$ mice).

[†]Tween 80 7%/3% ethanol formulation ($n \geq 10$ mice).

Fig. 3. Genomic tiling arrays identified shared mutations in the *pfatp4* gene (PFL0590c) in all drug-resistant parasites. **(A)** Distinct pairs of SNPs in *pfatp4* were detected in NITD678-R^{Dd2} clones #2 (blue) and #3 (orange). *P* values were calculated for all probes covering *pfatp4* and flanking regions; a spike in the *P* value reflects a difference in hybridization between the parental clone and the drug-selected clone, a hallmark of a SNP. Direct sequencing of *pfatp4* from each clone confirmed that these SNPs cause nonsynonymous changes in the coding region, indicated by the red boxes. **(B)** A 120-kb copy number variation covering 37 genes in chromosome 12 was detected in the genome of NITD678-R^{Dd2} clone #1. The *pfatp4* gene (asterisk) was contained within this amplification. Direct sequencing of *pfatp4* from this clone identified an additional nonsynonymous SNP at amino acid position 223 (G223R). This mutation was continuously observed throughout numerous sequencing reads of subcloned *pfatp4* PCR products of NITD678-R^{Dd2} clone #1, suggesting that the mutation occurred before the amplification event and, thus, resides in all *pfatp4* gene copies in the genome. **(C)** The three NITD609-R^{Dd2} clones showed no evidence of copy number variants; however, each clone contained nonsynonymous SNPs in *pfatp4* (clone#1, red; clone#2, blue; clone#3, orange).



NITD609 was efficacious at doses ($ED_{50/90/99} = 1.2, 2.7,$ and 5.3 mg/kg) lower than those of the reference antimalarial drugs chloroquine, artesunate, and mefloquine (table S7). A single oral dose of NITD609 at 100 mg/kg completely cleared a *P. berghei* infection in all treated mice, and a 50% cure rate was achieved with a single oral dose at 30 mg/kg (Table 1). Three daily oral doses of 50 mg/kg also afforded complete cure (table S8). At similar dosing regimens, none of the reference drugs tested could cure infection in this lethal malaria mouse model. To our knowledge, among the drug candidates currently in development, only the new-generation synthetic

peroxide compounds (e.g., OZ439) have been reported to have this level of curative activity upon single-dose oral administration (7). Considering NITD609 pharmacokinetic and pharmacodynamic properties, we speculate that sustained parasitemia reduction will be achievable at low doses in humans.

Drug resistance mediated by a P-type cation-transporter ATPase4. The rapid development of drug resistance has plagued malaria control programs in almost all endemic regions. In vitro selection of resistance is a powerful predictor of the molecular determinants used by parasites in field settings (23, 24). To evaluate the potential for drug resistance and gain insight into the mechanism of action, we applied drug pressure to a cultured clone of Dd2, a multidrug-resistant parasite strain believed to have a higher propensity to mutate (25) (fig. S3A). Six independent cultures were exposed to incrementally increasing sublethal concentrations of two compounds: NITD609 and the less potent derivative NITD678 (fig. S3, B and C). After 3 to 4 months of constant drug pressure, the IC₅₀ values had increased 7- to 24-fold (attaining a mean of 3 to 11 nM) for NITD609-selected parasites, and 7- to 11-fold (mean of 162 to 241 nM) for NITD678-selected parasites (fig. S3, D and E, and table S9). The high number of passages required to yield drug-resistant parasites, together with the low level of resistance that was achieved, suggests that spiroindolones do not readily select for high-level resistance in vitro. Subsequent passaging of drug-selected parasites in drug-free media for 4 months showed no evidence of revertants, indicating that resistance was stable (fig. S4). None of the selected mutants showed cross-resistance to a panel of antimalarial agents with diverse modes of action, including artemisinin and mefloquine (table S10).

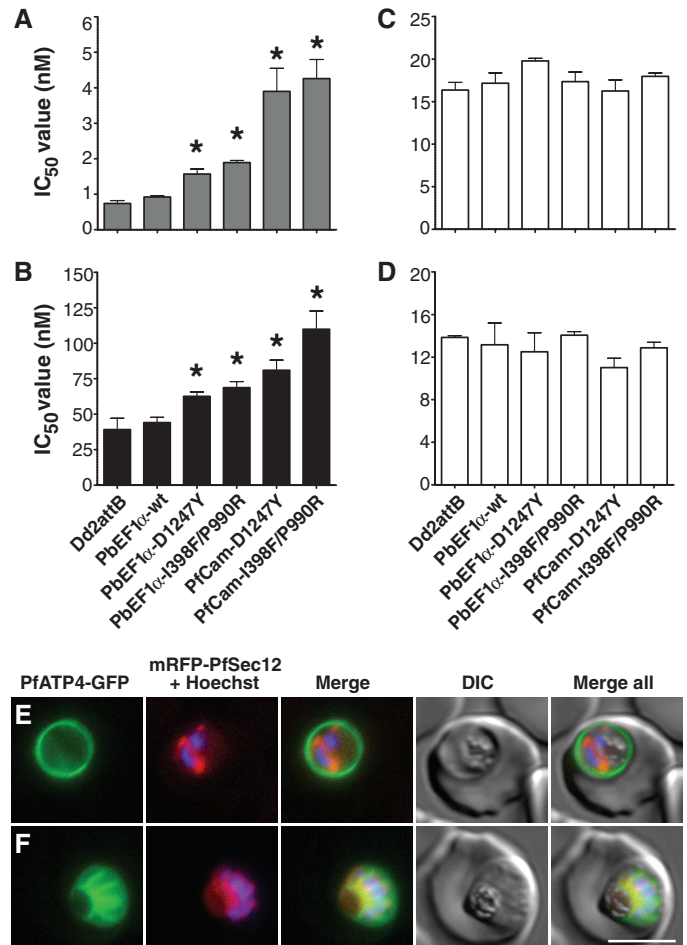
To determine the molecular basis of in vitro resistance, we prepared genomic DNA (gDNA) from each of the six drug-resistant clones. gDNA samples were then fragmented, labeled, and hybridized to a high-density tiling array that contains ~6 million single-stranded 25-oligonucleotide probes complementary to the *P. falciparum* genome. We compared the hybridization data for each haploid clone, using software that identifies regions on the array that showed a loss or gain of hybridization relative to the nonresistant parental reference line (26), and that calculated a probability of a genomic change based on the number of consecutive probes that showed a hybridization difference. The microarray covers ~90% of coding regions and 60% of noncoding regions, with probes spaced every two or three bases. Sequence coverage is limited only by the high AT content of *P. falciparum* that causes some 25-oligonucleotide sequences to be represented more than once throughout the genome, rendering those noninformative (27). Former studies showed that this genome-tiling analysis can identify 90% of the differences that distinguish two strains in unique regions of the genome (26).

Detectable genomic changes include single-nucleotide polymorphisms (SNPs), insertion/deletion events, and copy number variations. Using a permissive *P*-value cutoff of 1×10^{-5} , we identified 7 to 95 genomic differences, localized to within 2 or 3 nucleotides, in each resistant clone. A similar comparison between two highly diverged strains such as Dd2 and 3D7 would yield >13,000 genomic differences (26). Using a stricter cutoff ($P < 10^{-10}$) that should give fewer false-positives at the expense of more false-negatives, we found 27 total differences among all six mutants. Seven of these mapped to a single gene, *pfatp4* (PFL0590c; Fig. 3, A and C), with the remainder found largely in randomly assorted subtelomeric or intergenic regions. Inspection of the hybridization patterns showed that one strain carried a copy number variant that encompassed the *pfatp4* locus (Fig. 3B). These data strongly suggest that treatment with spiroindolones specifically selects for mutations in *pfatp4*.

Sequencing of the entire *pfatp4* gene from the different resistant strains revealed 11 non-

synonymous mutations (table S9), with at least one in every clone. Nine of these were considered true genomic alterations for the thresholds used with the microarray analysis ($P < 10^{-5}$). One exception resulted from a SNP lying within the copy number variant (NITD678-R^{Dd2} clone#1). The second exception (NITD609-R^{Dd2} clone#1) was the result of an emergent mixed population that had been cultured for several weeks after cloning in order to obtain enough DNA for hybridization. Sequencing of different polymerase chain reaction (PCR) products from this clone showed that some fragments contained three mutations (Ile³⁹⁸→Phe, Pro⁹⁹⁰→Arg, and Asp¹²⁴⁷→Tyr) in *pfatp4*, whereas others harbored only two mutations (Ile³⁹⁸→Phe and Pro⁹⁹⁰→Arg). The probability of 11 nonsynonymous mutations occurring in *pfatp4* by chance is extremely unlikely. Sequencing of 14 different isolates of *P. falciparum* from different continents (28, 29) revealed only 7 non-synonymous SNPs and 6 synonymous SNPs for *pfatp4* (from a total of ~32,000 SNPs), placing the gene at

Fig. 4. Introduction of mutant *pfatp4* into Dd2^{attB} parasites decreases susceptibility to spiroindolones. *pfatp4* transgenes harboring mutations identified in either NITD609-R^{Dd2} clone #1 (I398F/P990R) or clone #3 (D1247Y) were individually introduced into the parental Dd2 background to evaluate the ability of the mutant protein to protect against spiroindolone activity. As a control, wild-type *pfatp4* was also introduced. Expression of *pfatp4* was regulated by either the *P. berghei* EF1 α promoter (PbEF1 α) or the stronger *P. falciparum* calmodulin promoter (PfCam). IC₅₀ values were determined for (A) NITD609, (B) NITD678, (C) artemisinin, and (D) mefloquine. IC₅₀ values are shown as means \pm SD and were derived from three independent experiments performed in quadruplicate with the SYBR Green-based cell proliferation assay (12). Statistical significance was calculated using a two-tailed unpaired *t* test, comparing transgenic *pfatp4* lines to the Dd2^{attB} parental line: **P* < 0.0001. (E and F) Localization of PfATP4 to the parasite plasma membrane. Transgenic parasites coexpressing PfATP4-GFP and an ER marker, mRFP-PfSec12, were labeled with Hoechst 33382 to visualize the nucleus. PfATP4-GFP was observed at the parasite plasma membrane in (E) early schizont (two nuclei) and (F) late-segmented schizont parasites. DIC, differential interference contrast. Bar, 5 μ m.



about the 70th percentile in terms of diversity. In contrast, none of the genes with the highest number of nonsynonymous SNPs from sequencing field isolates (28, 29) showed any differences in our tiling array analysis. Thus, our data are indicative of selective pressure operating on this single gene.

To confirm that drug resistance was conferred directly by these mutations, we amplified the full-length *pfatp4* gene from either wild-type or resistant lines, and cloned it into an expression vector that allows for site-specific integration in transgenic parasites (fig. S5). Following integrase-mediated recombination (30) to introduce these genes stably into parasites, we evaluated transgenic lines for inhibition of parasite growth as a function of drug concentration. Lines expressing mutant PfATP4 harboring either the single Asp¹²⁴⁷→Tyr (D1247Y) or double Ile³⁹⁸→Phe/Pro⁹⁹⁰→Arg (I398F/P990R) mutations showed an increase in IC₅₀ values relative to the parental line (Fig. 4, A and B, and table S11). This effect was enhanced when either mutant was placed under the control of the strong *P. falciparum* calmodulin (PF14_0323) promoter, conferring a fivefold increase in the IC₅₀ value against NITD609. The reduced level of resistance compared to the original drug-selected mutants can be attributed to the coexpression of variant *pfatp4* and the endogenous wild-type allele in our transfected lines. Artemisinin (Fig. 4C) and mefloquine (Fig. 4D) displayed equivalent potency against the wild-type and transgenic strains (table S11), confirming that resistance was specific to the spiroindolones.

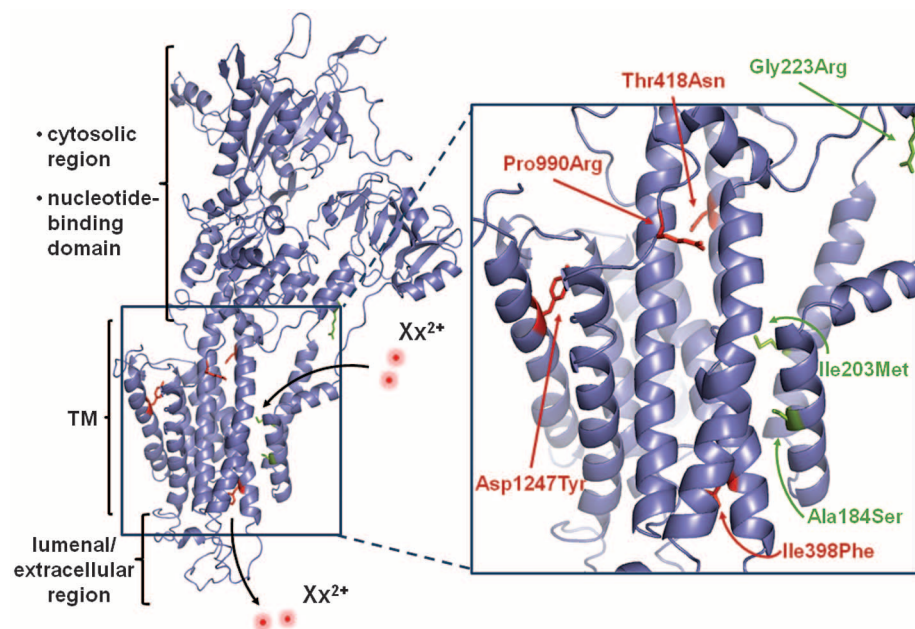


Fig. 5. Resistance-associated SNPs map to the predicted transmembrane region of PfATP4. A homology model of PfATP4 was generated in SWISS-MODEL based on the crystal structure of the rabbit SERCA pump. Amino acid alignment analysis by EMBOSS (43) revealed 30% identity and 48% similarity between these proteins. Residues corresponding to resistance-associated mutations are indicated in red for NITD609-R^{Dd2} and in green for NITD678-R^{Dd2}. These mutations mapped to the putative transmembrane (TM) helices. The sites of divalent cation entry and exit are indicated as Xx²⁺.

Molecular characterization of PfATP4. The *pfatp4* gene product is annotated as a cation-transporting P-type adenosine triphosphatase (ATPase) (PfATP4) (31–33). This family of ATP-consuming transporters can be inhibited by chemically diverse compounds, including thapsigargin, cyclopiazonic acid, and lansoprazole, and thereby constitutes an attractive set of drug targets [reviewed in (34)]. P-type ATPases are ubiquitous in eukaryotic organisms, and those involved in divalent cation transport appear to maintain a conserved structural mechanism for ion translocation (35). PfATP4 shows a high level of homology to *Saccharomyces cerevisiae* PMR1, a P-type ATPase required for high-affinity Ca²⁺ and Mn²⁺ transport. The human ortholog (hSPCA1) is associated with Hailey-Hailey disease, an acantholytic skin condition. The structural elucidation of a related rabbit SERCA (sarco/endoplasmic reticulum calcium ATPase) pump (36), which shares 30% amino acid identity with PfATP4, enabled us to generate a homology model (Fig. 5). This localizes most of the eight resistance-associated mutations to transmembrane domains. The transmembrane region is predicted to act as a funnel to translocate cations across biological membranes, and includes eight conserved residues required for cation coordination (37, 38). None of those residues were altered in our resistant lines. A number of P-type ATPase inhibitors, including cyclopiazonic acid and thapsigargin, bind to the transmembrane region (39–41). However, no cross-resistance to either inhibitor was observed in our spiroindolone-selected mutant parasite lines (table S10).

To characterize PfATP4 further, we generated a PfATP4-GFP (green fluorescence protein) fusion that was cotransfected into Dd2 parasites along with mRFP-PfSec12, an endoplasmic reticulum (ER) marker (42). Live cell imaging of transgenic parasites localized PfATP4-GFP to the parasite plasma membrane throughout the intraerythrocytic life cycle (Fig. 4, E and F, and fig. S6). In late-stage segmented schizonts, this fusion protein was invaginated and surrounded the developing daughter merozoites, confirming a parasite plasma membrane distribution rather than delivery to the surrounding parasitophorous vacuole (Fig. 4F). This finding is supported by earlier immunofluorescence data that localized PfATP4 at or near the plasma membrane (32).

Several possibilities may explain how mutations in PfATP4 could confer resistance to spiroindolones. First, the protein could play a role in drug transport; however it shows no homology to known transporters. Alternatively, PfATP4 mutations could attenuate the spiroindolone-induced disruption of cellular homeostasis through an indirect mechanism that remains to be determined. Finally, PfATP4 may be the target of spiroindolones because cation-transporting ATPases are druggable targets (34). It is difficult to distinguish between these possibilities as little is known about the molecular function of PfATP4. We have been unable to reproduce results suggesting that PfATP4 plays a role in calcium transport (33) (fig. S7), and it is unlikely that the protein regulates calcium transport of the ER calcium stores, given its localization to the plasma membrane. It is possible, nonetheless, that the protein regulates the trafficking of other cations. Although further functional characterization of PfATP4 is clearly warranted, the mutations we identified will be useful molecular markers of drug resistance once NITD609 enters clinical trials.

Conclusions. These studies define the spiroindolones as an antimalarial drug candidate that acts through a mechanism of action distinct from that of existing antimalarial drugs. In contrast to mefloquine and artemisinin, spiroindolones rapidly suppress protein synthesis in the parasite. Our genome-wide investigations revealed that resistance is mediated by the P-type ATPase PfATP4 and showed at single-base resolution how a small eukaryotic genome adapts to sublethal drug pressure. Our lead compound, NITD609, displays good antimalarial activity and meets the criteria required for an antimalarial drug candidate. Further safety and pharmacological preclinical evaluation is currently ongoing to support the initiation of human clinical trials.

References and Notes

1. WHO, World Malaria Report 2009; www.who.int/malaria/world_malaria_report_2009/en/.
2. B. M. Greenwood *et al.*, *J. Clin. Invest.* **118**, 1266 (2008).
3. R. T. Eastman, D. A. Fidock, *Nat. Rev. Microbiol.* **7**, 864 (2009).

4. A. M. Dondorp *et al.*, *N. Engl. J. Med.* **361**, 455 (2009).
5. H. Noedl *et al.*, *N. Engl. J. Med.* **359**, 2619 (2008).
6. N. J. White, *Science* **320**, 330 (2008).
7. P. Olliaro, T. N. Wells, *Clin. Pharmacol. Ther.* **85**, 584 (2009).
8. T. N. C. Wells, P. L. Alonso, W. E. Gutteridge, *Nat. Rev. Drug Discov.* **8**, 879 (2009).
9. E. A. Winzeler, *Nature* **455**, 751 (2008).
10. F. J. Gambo *et al.*, *Nature* **465**, 305 (2010).
11. W. A. Guiguemde *et al.*, *Nature* **465**, 311 (2010).
12. D. Plouffe *et al.*, *Proc. Natl. Acad. Sci. U.S.A.* **105**, 9059 (2008).
13. See supporting material on Science Online.
14. B. M. Russell *et al.*, *Antimicrob. Agents Chemother.* **47**, 170 (2003).
15. J. P. Guthmann *et al.*, *Trop. Med. Int. Health* **13**, 91 (2008).
16. N. J. White, *J. Antimicrob. Chemother.* **30**, 571 (1992).
17. W. W. Sharrock *et al.*, *Malar. J.* **7**, 94 (2008).
18. M. Traebert, B. Dumotier, *Expert Opin. Drug Saf.* **4**, 421 (2005).
19. N. J. White, *Lancet Infect. Dis.* **7**, 549 (2007).
20. B. N. Ames, F. D. Lee, W. E. Durston, *Proc. Natl. Acad. Sci. U.S.A.* **70**, 782 (1973).
21. D. A. Fidock, P. J. Rosenthal, S. L. Croft, R. Brun, S. Nwaka, *Nat. Rev. Drug Discov.* **3**, 509 (2004).
22. J. L. Vennerstrom *et al.*, *Nature* **430**, 900 (2004).
23. K. Hayton, X. Z. Su, *Curr. Genet.* **54**, 223 (2008).
24. A. Nzila, L. Mwai, *J. Antimicrob. Chemother.* **65**, 390 (2010).
25. P. K. Rathod, T. McErlean, P. C. Lee, *Proc. Natl. Acad. Sci. U.S.A.* **94**, 9389 (1997).
26. N. V. Dharia *et al.*, *Genome Biol.* **10**, R21 (2009).
27. M. J. Gardner *et al.*, *Nature* **419**, 498 (2002).
28. S. K. Volkman *et al.*, *Nat. Genet.* **39**, 113 (2007).
29. D. C. Jeffares *et al.*, *Nat. Genet.* **39**, 120 (2007).
30. L. J. Nkrumah *et al.*, *Nat. Methods* **3**, 615 (2006).
31. F. Trottein, J. Thompson, A. F. Cowman, *Gene* **158**, 133 (1995).
32. M. Dyer, M. Jackson, C. McWhinney, G. Zhao, R. Mikkelsen, *Mol. Biochem. Parasitol.* **78**, 1 (1996).
33. S. Krishna *et al.*, *J. Biol. Chem.* **276**, 10782 (2001).
34. L. Yatime *et al.*, *Biochim. Biophys. Acta* **1787**, 207 (2009).
35. W. Kühlbrandt, *Nat. Rev. Mol. Cell Biol.* **5**, 282 (2004).
36. A. M. Jensen, T. L. Sørensen, C. Olesen, J. V. Møller, P. Nissen, *EMBO J.* **25**, 2305 (2006).
37. D. M. Clarke, T. W. Loo, G. Inesi, D. H. MacLennan, *Nature* **339**, 476 (1989).
38. C. Toyoshima, M. Nakasako, H. Nomura, H. Ogawa, *Nature* **405**, 647 (2000).
39. C. Toyoshima, H. Nomura, *Nature* **418**, 605 (2002).
40. K. Moncoq, C. A. Trieber, H. S. Young, *J. Biol. Chem.* **282**, 9748 (2007).
41. M. Takahashi, Y. Kondou, C. Toyoshima, *Proc. Natl. Acad. Sci. U.S.A.* **104**, 5800 (2007).
42. M. C. Lee, P. A. Moura, E. A. Miller, D. A. Fidock, *Mol. Microbiol.* **68**, 1535 (2008).
43. P. Rice, I. Longden, A. Bleasby, *Trends Genet.* **16**, 276 (2000).
44. We thank A. Matter, M. Tanner, and P. Herrling for their foresight and support in establishing a malaria drug discovery program in the context of a public-private partnership. We thank T. A. Smith (SwissTPH) for the statistical analysis of the stage and rate of action studies. We thank S. Rao (Novartis Institute for Tropical Diseases) and M. Traebert (Novartis-preclinical safety), respectively, for the cytotoxicity and hERG inhibition data. We also thank M. Weaver (Novartis-preclinical safety) for the interpretation of the preclinical toxicology data. The team acknowledges P. Schultz, who had the vision to see the potential of the drug resistance experiments in the exploratory phase. In addition, we are grateful to R. T. Eastman for providing guidance to establish the in vitro drug-selection protocol and for providing the cloned Dd2 parasites. Finally, the scientific expertise provided by S. E. R. Bopp and S. K. Sharma and their helpful discussions throughout this project are greatly appreciated. Funding for the PfATP4 transfectants was provided to the Fidock laboratory in part by the Medicines for Malaria Venture (MMV08/0015; PI D. Fidock). The Shoklo Malaria Research Unit is sponsored by the Wellcome Trust of Great Britain, as part of the Oxford Tropical Medicine Research Programme of Wellcome Trust—Mahidol University. Laurent Renia's laboratory is supported by a core grant from the Singapore Immunology Network, A*STAR. This work was supported by a grant from the Medicines for Malaria Venture and a translational research grant (WT078285) from the Wellcome Trust to the Novartis Institute for Tropical Diseases, the Genomics Institute of the Novartis Research Foundation and the Swiss Tropical Institute, and by grants to E.A.W. from the W. M. Keck Foundation and the NIH (R01AI059472). NITD609 is described in the Novartis patent application WO2009/132921. All requests for spiroindolones or related compounds are subject to a Material Transfer Agreement. T.H.K. and E.A.W. own shares in Novartis (Switzerland).

Supporting Online Material

www.sciencemag.org/cgi/content/full/329/5996/1175/DC1
Materials and Methods
Figs. S1 to S10
Tables S1 to S13
References

3 June 2010; accepted 30 June 2010
10.1126/science.1193225

REPORTS

Detection of C₆₀ and C₇₀ in a Young Planetary Nebula

Jan Cami,^{1,2*} Jeronimo Bernard-Salas,^{3,4} Els Peeters,^{1,2} Sarah Elizabeth Malek¹

In recent decades, a number of molecules and diverse dust features have been identified by astronomical observations in various environments. Most of the dust that determines the physical and chemical characteristics of the interstellar medium is formed in the outflows of asymptotic giant branch stars and is further processed when these objects become planetary nebulae. We studied the environment of Tc 1, a peculiar planetary nebula whose infrared spectrum shows emission from cold and neutral C₆₀ and C₇₀. The two molecules amount to a few percent of the available cosmic carbon in this region. This finding indicates that if the conditions are right, fullerenes can and do form efficiently in space.

Interstellar dust makes up only a small fraction of the matter in our galaxy, but it plays a crucial role in the physics and chemistry of the interstellar medium (ISM) and star-forming regions (1). The bulk of this dust is created in the outflows of old, low-mass asymptotic giant branch (AGB) stars; such outflows are slow (5 to 20 km/s) but massive (10⁻⁸ to 10⁻⁴ solar masses per year)

(2–4). Once most of the envelope is ejected, the AGB phase ends and the stellar core—a hot white dwarf—becomes gradually more exposed. When this white dwarf ionizes the stellar ejecta, they become visible as a planetary nebula (PN).

Chemical reactions and nucleation in the AGB outflows transform the atomic gas into molecules and dust grains. For carbon-rich AGB stars (sometimes called carbon stars), this results in a large variety of carbonaceous compounds; to date, more than 60 individual molecular species and a handful of dust minerals have been identified in these outflows (5), including benzene, polynes, and cyanopolynes up to about 13 atoms in size (6, 7).

These environments are also thought to be the birthplace for large aromatic species such as

polycyclic aromatic hydrocarbons (PAHs) and fullerenes (8, 9), a class of large carbonaceous molecules that were discovered in laboratory experiments aimed at understanding the chemistry in carbon stars (10). Fullerenes have unique physical and chemical properties, and the detection of fullerenes and the identification of their formation site are therefore considered a priority in the field of interstellar organic chemistry (11). However, astronomical searches for fullerenes in interstellar and circumstellar media have not resulted in conclusive evidence (12–14). The most promising case to date is the detection of two diffuse interstellar bands (DIBs) in the near-infrared (15) whose wavelengths are close to laboratory spectra of C₆₀⁺ in solid matrices (16); this finding awaits confirmation from comparison to a cold, gas-phase spectrum.

Here, we report on the detection of the fullerenes C₆₀ and C₇₀ in the circumstellar environment of Tc 1. Tc 1 is a young, low-excitation PN where the white dwarf is still enshrouded by the dense stellar ejecta. At optical wavelengths, Tc 1 shows H α emission up to ~50 arc sec away from the central star, but the PN also has a much smaller (~9 arc sec) and more compact core that was observed with the Infrared Spectrograph (IRS) (17) onboard the Spitzer Space Telescope (18). This inner region turns out to be carbon-rich, hydrogen-poor, and dusty.

The Spitzer IRS spectrum of Tc 1 (Fig. 1) (19) shows numerous narrow forbidden emission

¹Department of Physics and Astronomy, University of Western Ontario, London, Ontario N6A 3K7, Canada. ²SETI Institute, 515 North Whisman Road, Mountain View, CA 94043, USA. ³222 Space Sciences Building, Cornell University, Ithaca, NY 14853, USA. ⁴Institut d'Astrophysique Spatiale, CNRS/Université Paris-Sud 11, 91405 Orsay, France.

*To whom correspondence should be addressed. E-mail: jcam@uwo.ca